frontiers in Earth Science

ORIGINAL RESEARCH
published: 21 March 2022
doi: 10.3389/feart.2022.865322

Geochemical Characteristics of Rare Earth Elements in the Chaluo Hot Springs in Western Sichuan Province, China

Shuaichao Wei[1,2], *Feng Liu*[1,2,3], *Wei Zhang*[1,2]*, *Hanxiong Zhang*[1,2], *Rouxi Yuan*[1,2], *Yuzhong Liao*[1,2] *and Xiaoxue Yan*[1,2]

[1]*The Institute of Hydrogeology and Environmental Geology, Chinese Academy of Geological Sciences, Shijiazhuang, China,* [2]*Technology Innovation Center of Geothermal and Hot Dry Rock Exploration and Development, Ministry of Natural Resources, Shijiazhuang, China,* [3]*China University of Geosciences (Beijing), Beijing, China*

OPEN ACCESS

Edited by:
Dawei Hu,
Institute of Rock and Soil Mechanics (CAS), China

Reviewed by:
Qixin Wu,
Guizhou University, China
Santosh Kumar Rai,
Wadia Institute of Himalayan Geology, India

***Correspondence:**
Wei Zhang
18879003@qq.com

Specialty section:
This article was submitted to Geochemistry, a section of the journal Frontiers in Earth Science

Received: *29 January 2022*
Accepted: *02 March 2022*
Published: *21 March 2022*

Citation:
Wei S, Liu F, Zhang W, Zhang H, Yuan R, Liao Y and Yan X (2022) Geochemical Characteristics of Rare Earth Elements in the Chaluo Hot Springs in Western Sichuan Province, China. Front. Earth Sci. 10:865322. doi: 10.3389/feart.2022.865322

High-temperature hydrothermal activity areas in western Sichuan Province, China are ideal objects for studying deep Earth science, extreme ecological environments, and comprehensive geothermal utilization. To understand the geochemical characteristics of rare Earth elements (REEs) in the Chaluo hot springs in western Sichuan Province, the authors analyzed the composition and fractionation of REEs in the hot springs through hydrochemical analysis, REE tests, and North American Shale Composite-normalized REE patterns. Moreover, the composition and complex species of REEs in the geothermal water in the Chaluo area were determined through calculation and simulation analysis using the Visual MINTEQ 3.0 software. The results are as follows. In terms of hydrochemical type, all geothermal water in the Chaluo area is of the Na-HCO_3 type. The cations in the geothermal water are mainly controlled by water-rock interactions and evaporation, the anions are determined by water-rock interactions, and the hydrochemical processes are primarily controlled by the dissolution of silicate minerals. The total REE content of the geothermal water in the Chaluo hot springs is 0.306 ± 0.103 ug/L. It is low compared to the Kangding area and is primarily affected by the reductive dissolution of Fe oxides/hydroxides, followed by pH. The geothermal water in the Chaluo area is rich in light rare Earth elements (LREEs) because of the presence of Fe oxides. It shows positive Eu and Ce anomalies due to the combined effects of the dissolution of Eh and Mn oxides and surface water. Furthermore, the positive Eu anomalies are also caused by the water-rock interactions between the Qugasi Formation and deep geothermal water. Similar to alkaline water bodies, the complex species of REEs in the geothermal water mainly include $Ln(CO_3)_2^-$, $LnCO_3^+$, and $LnOH^{2+}$, which is caused by the stability constants of complexation reactions.

Keywords: Chaluo hot springs, rare earth elements, North American shale standardized REE distribution patterns, Eu anomaly, complexes of the species

INTRODUCTION

Western Sichuan Province is located at the easternmost end of the Mediterranean-Himalayan geothermal zone and at the boundary of the collision between the Eurasian Plate and the African and Indian plates (Royden et al., 2008; Xu et al., 2011; **Figure 1A**). This region is mainly composed of three strike-slipping faults-the Xianshuihe, Ganzi-Litang, and Jinshajiang faults (Dewey et al., 1988; Xu et al., 2005; Yan and Lin, 2015), the Songpan-Ganzi fold belt, and the Yidun arc (SBGMR, 1991; Xu et al., 1992; Zhang et al., 2013; Tang et al., 2017; **Figure 1B**). It is characterized by strong neotectonic movements, frequent earthquakes, active hot springs, and geothermal anomalies (Tang et al., 2017; Zhang Jian. et al., 2017). Statistics reveal that 248 hot springs are distributed in this region (Luo, 1994). Similar to the Yangbajing geothermal field in Tibet and the Rehai geothermal field in Tengchong City, Yunnan Province (Tong et al., 1981; Tong and Zhang, 1989), the high-temperature geothermal resources in western Sichuan Province have various geothermal manifestations including geysers, boiling springs, and boiling spouters, hydrothermal explosions, and hydrothermal alterations (Fan et al., 2019; **Figure 1B**). The hot springs in western Sichuan Province are mainly controlled by the Jinshajiang, Dege-Xiangcheng, Ganzi-Litang, and Xianshuihe faults in the giant structure in the shape of Chinese character "歹", which reach as deep as the Moho (Zhang Jian. et al., 2017; **Figure 1B**). Medium- and high-temperature hot springs are intensively exposed in the Kangding, Batang, and Litang areas. They exhibit strong hydrothermal activities, bear rich high-temperature thermal energy, and therefore have considerable potential for geothermal resource development (Fu and Yin, 2009). These high-temperature hydrothermal activity areas, which are ideal for understanding deep Earth science, extreme ecological environments, and the comprehensive utilization of geothermal energy, have attracted the attention of domestic and foreign experts and researchers in geothermal, geological, geochemical, and ecological fields.

Previous hydrogeochemical studies on the hot spring system in western Sichuan Province have mainly focused on the material origin and the recharge, runoff, and discharge conditions of hot springs, the characteristics and genetic mechanisms of geothermal reservoirs, and the structure, formation, and evolution of crust-mantle heat flow (Zhang Jian. et al., 2017; Yuan et al., 2017; Zhang Y. et al., 2018; Li et al., 2018; Zhang et al., 2019; Cao et al., 2021). Zhao J. Y. et al. (2019) analyzed the evolution of geothermal water in the Batang area by calculating the thermal storage temperature, cold water mixing ratio, and thermal circulation depth. Cao et al. (2021) studied the recharge sources, recharge elevation, geothermal water circulation depth, and geothermal storage temperature of the Chaluo geysers. Yuan et al. (2017) concluded that the differences in hydrochemical characteristics in western Sichuan Province are primarily caused by the dissolution and precipitation of minerals and cation exchanges. Previous research methods are mostly limited to traditional water chemistry and hydrogen and oxygen isotopes, and lack of combined analyses of macronutrients, trace elements and rare Earth elements, which make it difficult to accurately reflect the complex hydrogeochemical evolution of water-rock processes in deep and large fractured geothermal systems. Therefore, the combined hydrochemical and rare-earth element analyses are used in this study to provide a more detailed picture of the water-rock interaction in hot springs.

REEs consist of a group of elements with similar physicochemical properties (Hederson, 1984). They generally do not break in geochemical processes and thus have been widely used to trace the processes such as water-rock interactions in surface water (Goldstein and Jacobsen, 1988; Ménager et al., 1992; Johannesson et al., 1997; Dia et al., 2000; Göb et al., 2013). However, there are relatively few studies on the application of REEs in geothermal systems (Möller, 2000; Wood and Shannon, 2003; Sanada et al., 2006). Since REEs serve as a valuable tool for retrospectively studying the origin of geothermal fluids, the study of REEs is fundamental to understanding fluid-rock systems. Therefore, it is necessary to study the geochemical characteristics of REEs in geothermal fluids to improve the understanding of the behavior of geothermal fluids. This study analyzed the composition, fractionation, and key affecting factors of REEs in the geothermal system in the Chaluo hot springs. It will improve the understanding of the genesis of the geothermal system and provide guidance for increasing the development and utilization efficiency of local geothermal resources.

REGIONAL GEOTHERMAL GEOLOGICAL CHARACTERISTICS

The study area is located in the Jinshajiang fault and has cut downward to the upper mantle (Zhang Jian. et al., 2017; Zhang, 2020). In this area, the Late Yanshanian-Himalayan faults are superimposed on the earlier tectonic traces and cut through earlier structures. As a result, a checkerboard structural pattern with obvious fracture zones and fracture surfaces has been formed, providing favorable channels for the recharge and runoff of geothermal water. Meanwhile, the checkerboard structural pattern noticeably restricts hydrothermal activities, and the hot springs mostly spread along the fracture zones. By contrast, Indonesian structures in the study area are long and deep. They control the magmatic activities in the area and further control deep hydrothermal convection in the study area. The intersections of these structures of different eras show intensive high-temperature hydrothermal activities. The Rekeng and Reshuitang hot springs in Chaluo Town investigated in this study are also located at the intersections.

The study area lies in a hilly plateau subject to tectonic erosion. The mountains show high-grade slopes, and valleys are wide and gentle, with middle and lower parts downcutting deeply. The height differences between mountain peaks and valley bottom are generally less than 500 m. The rainfall in the Batang area is low and shows an uneven spatial-temporal distribution. It is mainly concentrated from June to September, with an average annual rainfall of 474 mm (Zhang, 2020). The Baqu River with plenty and stable water is the main river in the study area. It is a first-order tributary of the Jinsha River, with a length of 144 km and an annual runoff of about 800 million m^3. It is mainly recharged by precipitation and a small amount of snowmelt.

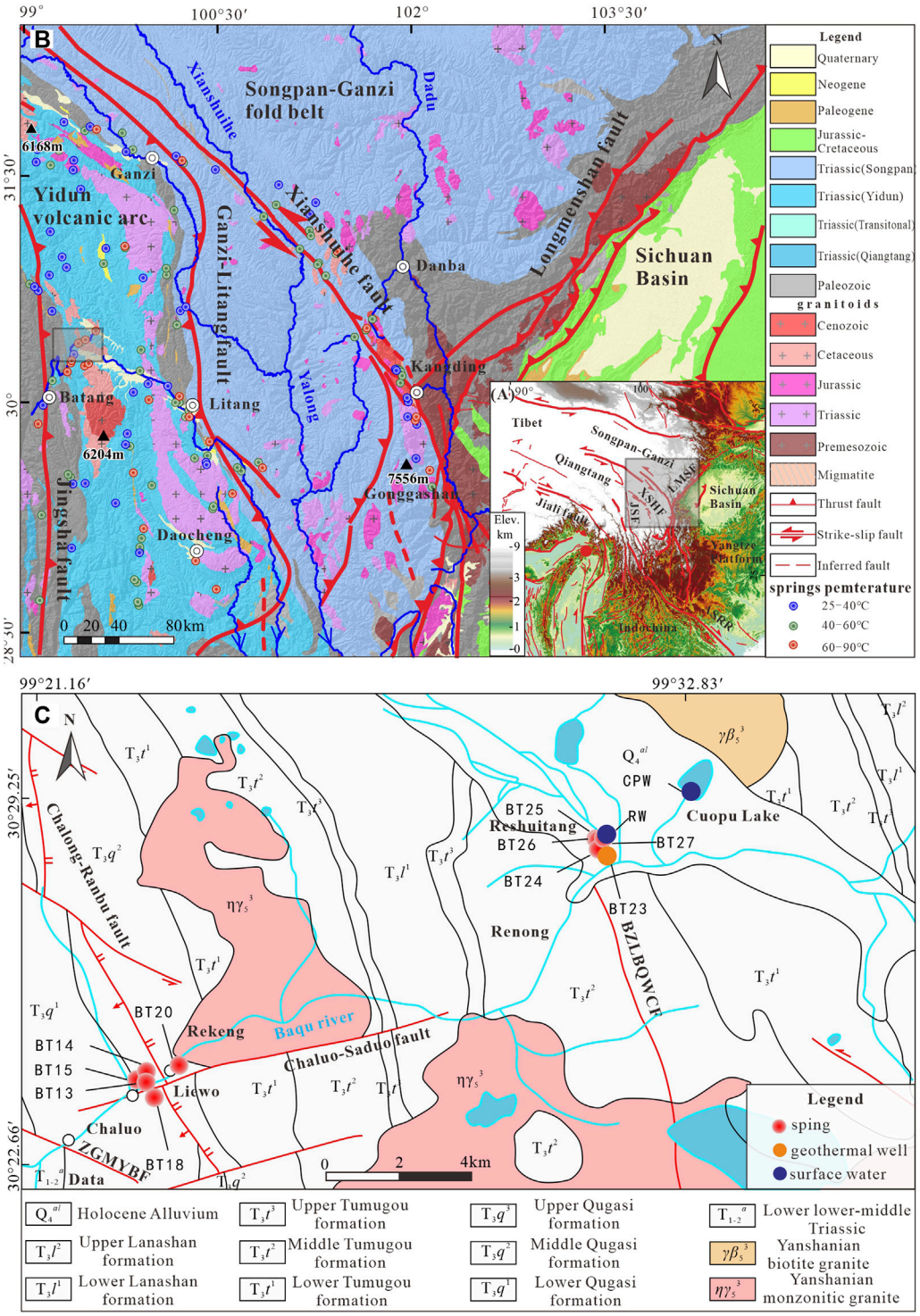

FIGURE 1 | (A) Topographic map of southwest China; **(B)** Geological map of the southeastern margin of the Tibetan Plateau (according to Zhang Y.-Z. et al., 2017; Tang and Johnnesson, 2010). **(C)** Geological map of the Chaluo area, Batang County, western Sichuan Province.

The study area features stratigraphic discontinuity, where Mesozoic strata dominated by Triassic strata (especially Upper Triassic strata) are widely distributed and outcrops also include Yanshanian biotite granites and monzonitic granites (**Figure 1C**). Hot springs in the study area are exposed in the Triassic Tumugou and Qugasi formations. The Qugasi Formation

FIGURE 2 | Field photo of Chaluo hot spring. **(A)** Hot pit spring mouth lower development of spring water; **(B)** Hot pit boiling spring waterfall; **(C)** Hot pit boiling spring; **(D)** Hot water pond boiling spring; **(E)** Geothermal well near hot water pond; **(F)** Baqu River water.

(T_3q) is exposed in the central part of the study area and spreads along Chaluo and Leiwo villages in the NS direction. With the Chalong-Ranbu fracture as a boundary, the Qugasi Formation can be roughly divided into the upper and lower members (**Figure 1C**). The upper member (T_3q^2) has a thickness of 2,295 m and is mainly composed of miscellaneous quartz conglomerates, sandy slates, slates, and dolomitic crystalline tuffs. Meanwhile, lamellibranchia and ammonite fossils occur in this member. The lower member (T_3q^1) has a thickness of 1,558 m. It is composed of light gray—dark gray crystalline tuffs, metamorphic sandstones, and slates and is interbedded with quartz conglomerates. The fossils occurring in this member include lamellibranchia, brachiopoda, and coral. The Tumugou Formation (T_3t), which is widely distributed in the study area, is a set of intermediate-acidic volcanic-sedimentary rock assemblages consisting of neritic-facies volcanic conglomerates, metamorphic sandstones, argillaceous argillites, and crystalline tuffs containing various types of volcanic conglomerates. This formation is in conformable contact with the overlying Lanashan Formation. It can be divided is divided into the upper, middle, and lower members. The upper member (T_3t^3) of the formation has a thickness of 972–4,832 m and is composed of sandstones and slates interbedded with intermediate and basal volcanic rocks and crystalline tuffs. The middle member (T_3t^2) has a thickness of 579–4,852 m. It is composed of interlayers with different thicknesses consisting of grayish-black lithic feldspar-quartz sandstones and dark slates, interbedded with rhyolites and limestones. The lower member (T_3t^1) has a thickness of 1,830 m and is composed of metamorphic sandstones and argillites. It bears conglomerates in most phase zones and is interbedded with acidic volcanic rocks locally. Moreover, it is in unconformable contact with the underlying strata in local areas.

The Chaluo hot springs refer to a group of hot springs distributed along both sides of the Baqu River in the NE direction from Chaluo Town to the Cuopu Lake in Batang County. They are mainly affected by the Zamagang-Maoyaba, Biezonglongba-Quwengcuo, Chaluo-Saduo, and Chalong-Ranbu faults (Zhang, 2020) and are mostly distributed in the shape of bands along the fault zones in the low-lying areas of the river valley, especially in the area between the Rekeng and Reshuitang areas (**Figure 1C**).

The hot springs in the Rekeng area (also referred to as the Rekeng hot springs) occur as a spring group. Their water mostly violently boils since its temperature is higher than the local boiling point (89°C; Cao et al., 2021). The hot and boiling springs have temperatures of 80–89°C and their fumaroles have a temperature of up to 99°C. The Rekeng hot springs are composed of more than a thousand springs in an area with a length of about 1,000 m, a width of 100–200 m, and an area of 0.15 km^2. Their outlets are mainly composed of strongly weathered zones consisting of elluvium-proluvium, pebble gravel, and bedrock. A large amount of calcareous tufa occurs below the outlets (**Figure 2A**), and its surrounding rocks are oxidized and brown. Meanwhile, a large area of tufa waterfalls is also present below the spring outlets (**Figure 2B**), with a height of about 50 m and a maximum thickness of 3 m. Local geothermal manifestations include boiling spouters, many boiling springs,

fumaroles, steaming ground, hot springs, and geysers (**Figure 2C**).

The hot springs in the Reshuitang area (also referred to as the Reshuitang hot springs) are also present as a spring group. Their temperatures are 27°C–89°C dominated by 80°C–87°C, mostly exceeding the local boiling point. These hot springs are primarily located on the high platform of a floodplain. The platform is made of calcareous tufa and spreads in the EW direction in the shape of an oval with a long axis of about 250 m and a short axis of about 150 m in length. The top of the platform is about 10 m above the water level. Hot and boiling springs are concentrated in an area of about 100 × 60 m^2 in the upper part of the high platform. They are composed of more than one hundred springs, each of which shows small water bubbles at dozens of positions. In addition, a few springs are distributed along the edge of the river valley. The surface geothermal manifestations include boiling spouters, many boiling springs, fumaroles, bubbling ground, and hot springs (**Figure 2D**). They are accompanied by a large amount of gas overflow and a small amount of H_2S odors, with milky white calcified sediments occurring in surrounding areas. In addition, geothermal wells (**Figure 2E**) and the Baqu River (**Figure 2F**) are also distributed near the Reshuitang hot springs.

SAMPLING AND TESTS

Samples were collected in September 2016. They include 10 samples collected from the Rekeng and Reshuitang hot springs in the area from Chaluo Village to the Cuopu Lake, one geothermal water sample and some core samples taken from the geothermal well next to the Reshuitang hot springs (the geothermal well was subsumed into the Reshuitang hot spring system), and two surface water samples collected from the Cuopu Lake and the Baqu River. The pH, Eh, total dissolved solids (TDS), and temperature of water were measured on site using portable water quality analyzers. 500 ml polyethylene bottles were used to collect the water samples after being cleaned and rinsed. The hydrochemical analysis of the water samples was conducted at the Key Laboratory of Groundwater Science and Engineering of the Ministry of Natural Resources, the Institute of Hydrogeology and Environmental Geology, Chinese Academy of Geological Sciences. The REE content of the water and rock samples was determined at the Central South Mineral Resources Supervision and Testing Center, Ministry of Land and Resources. The water samples used for tests of cations, trace elements, and isotopes were acidized until their pH was <2 by adding some drops of concentrated hydrochloric acid, while water samples used for anion tests were not acidified. Before tests, hydrochloric acid was added into the water samples using the titration method to eliminate the impacts of microorganisms and other impurities. Cations, anions, and trace elements were determined primarily using ICP-MS as per GB/TB 538-2008 Methods for examination of drinking natural mineral water. The REE contents of the water samples were tested using a plasma mass spectrometer, with analytical accuracy of better than 5%.

RESULTS AND DISCUSSION

Hydrochemical Characteristics

The hydrochemical compositions of the water samples are shown in **Table 1**. The Schöeller diagram (**Figure 3**) can be used to reflect the physicochemical properties of geothermal water from hot springs and geothermal wells and surface water from lakes and rivers. The geothermal water is neutral to alkaline and surface water is alkaline, and they have similar chemical compositions. However, the geothermal water contains higher concentrations of major ions, especially Na ions, than the surface water (**Figure 3**). The TDS content of the surface water and the geothermal water is 75.61–98.98 mg/L and 305.5–1,179 mg/L, respectively. For most water samples, the anions are dominated by HCO_3^-, and their contents are in the order of $HCO3- > SO42- > Cl-$. Meanwhile, cations in the water samples mainly included Na+, and their contents are in the order of $Na+ > K+ > Ca2+ > Mg2+$. The total dissolved cations ($TZ+ = Na+ + K+ 2Mg2+ + 2Ca2+$) and total dissolved anions ($TZ- = Cl- +2SO42- +HCO3- +2CO32-$) are well balanced: all samples have normalized inorganic charge balance, $NICB = (TZ+ - TZ-)/TZ+$, and all samples have NICB ≤10% (**Table 1**) (Moon et al., 2007). The Piper diagram of the water samples (Piper, 1994; **Figure 4**) illustrates the distribution of these cations and anions and the hydrochemical classification of the water samples. According to this diagram, three hydrochemical types were identified. All the geothermal water is of Na-HCO_3 type, the river water is of the mixed Ca-Na-HCO_3 type, and lake water is of Ca-HCO_3 type. Moreover, the greater concentrations of major ions and the higher TDS content in the geothermal water indicate a longer retention time and stronger water-rock interactions of the geothermal water (Zhang Y. et al., 2018).

Hydrochemical Processes

Soluble ions in water originate from various natural processes, such as precipitation, water-rock interactions, and evaporation, and these different processes can be distinguished using Gibbs diagrams (Gibbs, 1970). In the Gibbs diagram of TDS versus $Na^+/(Na^+ + Ca^{2+})$ and $Cl^-/(Cl^- + HCO^{3-})$ of the geothermal water (**Figure 5**), the $Na^+/(Na^+ + Ca^{2+})$ ratio is 0.87–0.99, falling in the zones of water-rock interactions and evaporation. Meanwhile, the $Cl^-/(Cl^- + HCO_3^-)$ ratio of the geothermal water is 0.05–0.17, falling into the water-rock interaction zone. These results indicate that cations in the geothermal water are mainly controlled by water-rock interactions and evaporation, while the anions in the geothermal water are dominated by water-rock interactions. The surface water samples fall in the water-rock interaction zone in the Gibbs diagram (**Figure 5**), indicating that the hydrochemical composition of the surface water is controlled by water-rock interactions.

The hydrochemical processes of water-rock interactions can be reflected from the correlation between the anion and cation

TABLE 1 | Hydrochemical composition of water samples in the study area (mg/L).

Sample	Location	T(°C)	Eh(mv)	pH	K^+	Na^+	Ca^{2+}	Mg^{2+}
BT13	Rekeng	89	−514.5	9.18	34.53	358.9	1.34	0.02
BT14	Rekeng	89	−574	9.27	29.81	317	0.81	0.013
BT15	Rekeng	90	−413.4	8.43	27.62	290.8	4.02	0.21
BT18	Rekeng	89	−517	8.97	28.86	343.8	0.65	0.013
BT20	Rekeng	53	45.1	8.26	2.41	90.24	11.61	0.81
BT23	Reshuitang	86	−550	8.19	26	353.2	6.41	2.92
BT24	Reshuitang	90	−442.1	9.1	26.23	351.6	0.77	0.1
BT25	Reshuitang	90	55.8	7.76	26.8	358.2	1.67	0.2
BT26	Reshuitang	90	64.8	8.03	25.24	345.2	0.8	0.1
BT27	Reshuitang	70	45.3	7.64	30.51	380.4	7.77	2.51
CPH	Cuopu Lake	15	75	8.96	0.75	0.65	19.55	1.81
RW	Baqu River	13	90	8.2	2.3	14.71	10.95	2.51

Sample	Cl^-	SO_4^{2-}	HCO_3^-	CO_3^{2-}	TDS	NICB[a] (%)	Fe	Mn
BT13	19.19	32.84	379.1	222.5	1,079	10	0.242	0.032
BT14	39.1	30.17	365	194.2	991.2	2.79	0.012	0.032
BT15	42.65	42.06	617.5	42.09	909	−0.21	0.021	0.032
BT18	51.9	25.45	428	180.4	1,041	4.48	0.012	0.001
BT20	8.89	20.74	217	—	305.5	8.50	0.036	0.006
BT23	33.77	19.47	904.9	18.04	1,071	−1.21	0.17	0.011
BT24	23.1	20.3	679.3	114.3	1,039	−0.03	0.425	0.009
BT25	33.77	42.62	885.9	—	1,071	0.04	0.381	0.004
BT26	33.06	42.09	862.1	—	1,033	−1.46	0.512	0.009
BT27	32.7	25.9	1,015	—	1,179	−0.98	0.016	0.01
CPH	1.78	22.89	42.8	—	75.61	−4.80	0.01	0.004
RW	1.78	17.95	61.75	—	98.98	1.08	0.162	0.003

[a]*NICB, normalized inorganic charge balance = $(TZ^+–TZ^-)/TZ^+ \times 100\%$.*

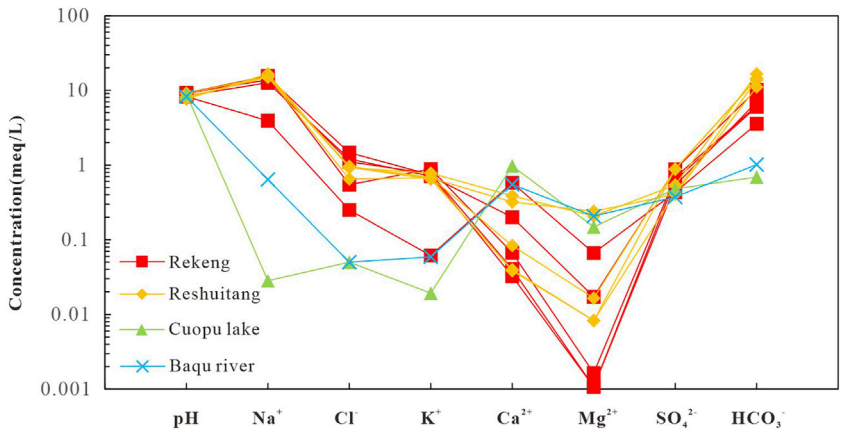

FIGURE 3 | Schöeller's diagram for different water samples in the study area.

contents (Li et al., 2020). According to the lithology of the strata in the study area, the rock formations contain minerals such as silicates, carbonates, sulphates and halides, and the main ions in the water samples originate from the dissolution of these minerals. Among these ions, Cl^- is rarely altered by water-rock interactions and mineral adsorption, even under high temperature and pressure conditions. Therefore, the correlation between Cl^- and other ions can account for the hydrochemical process in the geothermal water cycle (Li et al., 2020). If Na^+ is derived from halite dissolution, the molar ratio of Na^+ to Cl^- should be 1:1. **Figure 6A** shows that the surface water samples are distributed near the origin of coordinates in which the Na^+/Cl^+ ratios for CPW and RW were 0.56, 12.74 respectively. While the geothermal water shows a Na^+/Cl^- molar ratio of much higher than 1, implying that the excess Na^+ in the geothermal water may originate from silicate weathering (Zhang Y. et al., 2018). Ca^{2+} and SO_4^{2-} in groundwater are affected by the dissolution and precipitation of gypsum. If merely gypsum dissolves and precipitates in groundwater, as shown in **Eq. 1**, the molar ratio of Ca^{2+} to SO_4^{2-} should be 1:1. In the plot of Ca^{2+}

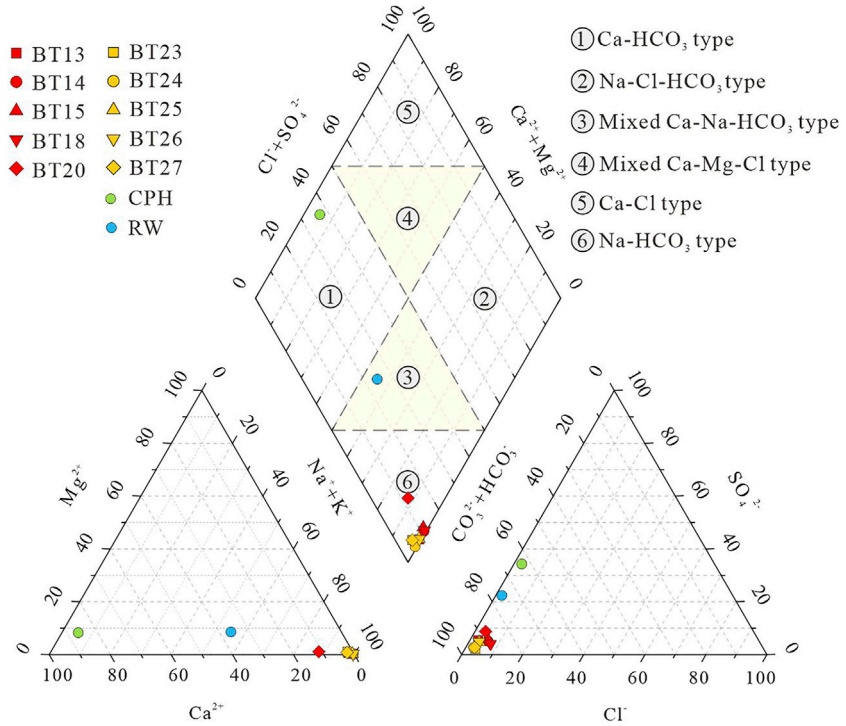

FIGURE 4 | Piper plot of water samples (modified from Piper, 1994; Zhang Y. et al., 2018).

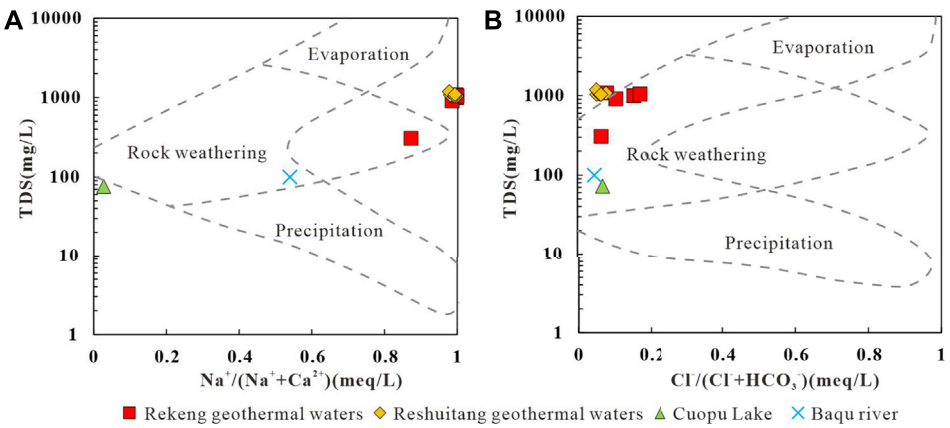

FIGURE 5 | Gibbs illustration of water samples in the study area. Rock weathering: the hydrochemical composition within the region is mainly influenced by rock weathering and dissolution; Evaporation: the hydrochemical composition within the region is mainly influenced by evaporation and concentration; Precipitation: the hydrochemical composition within the region is mainly influenced by atmospheric precipitation factors.

versus SO_4^{2-} (**Figure 6B**), only a few geothermal water and river water samples are distributed along the line with a slope of 1:1, and most of the geothermal water samples fall below the line with a slope of 1:1. These results indicate that the excess Ca^{2+} may originate from the dissolution of carbonate and silicate minerals. In addition, the relatively high SO_4^{2-} of some samples from the geothermal water and the Cuopu Lake may be influenced by human activities (Zhang Y. et al., 2018).

If the molar ratio of Ca^{2+} to HCO_3^- is 1:2, Ca^{2+} in groundwater originates from the dissolution of carbonate minerals (**Eq. 2**; Guo et al., 2020). In the plot of Ca^{2+} versus HCO_3^- (**Figure 6C**), the samples of river water and Cuopu Lake are distributed along the line with a slope of 1:2, and the molar ratio of Ca^{2+} to HCO_3^- of samples from the geothermal water are much less than 1:2. These results indicate that the Ca^{2+} in the geothermal water are derived from the dissolution of silicate minerals, while the Ca^{2+} in the

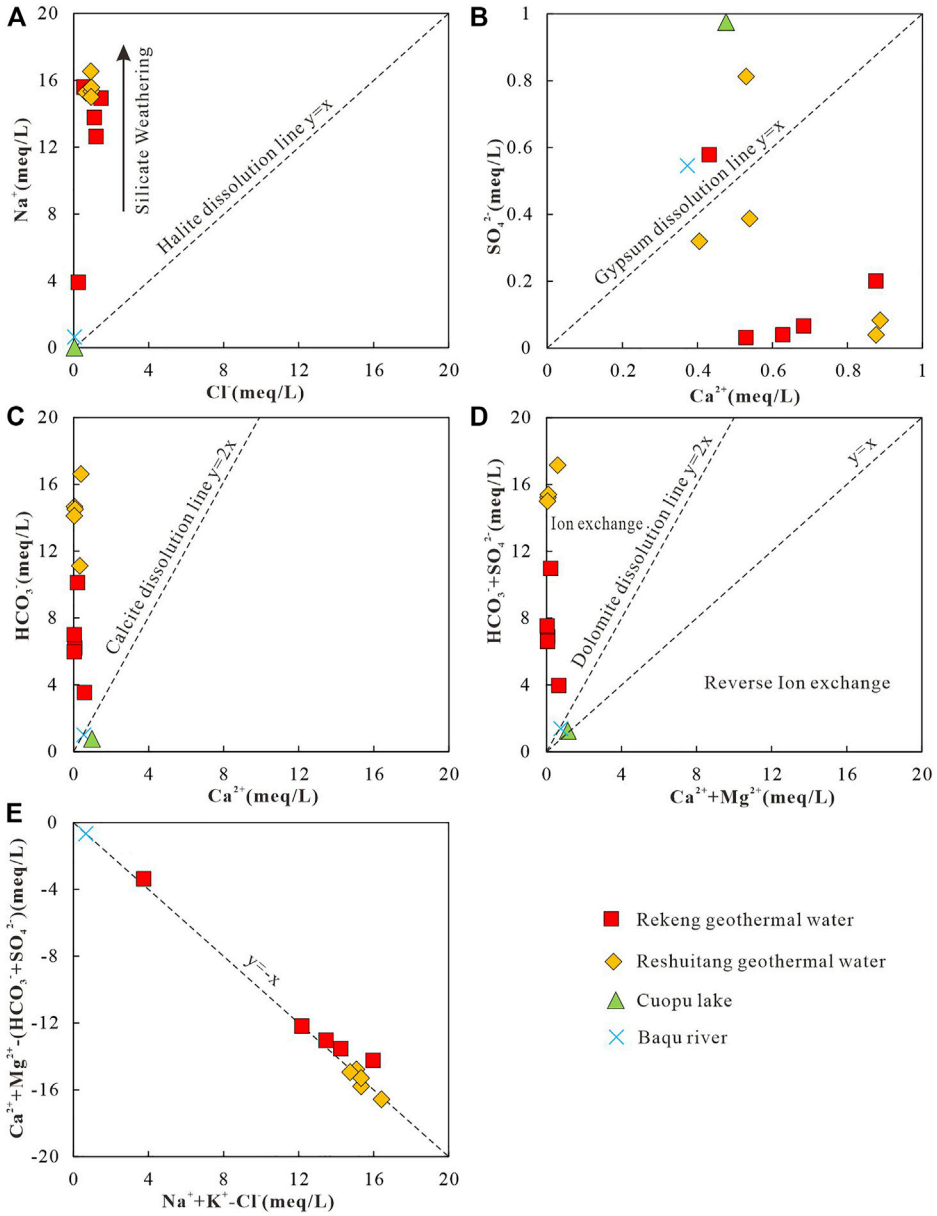

FIGURE 6 | Diagram of the determination of hydrochemical processes based on the molar ratio among the main ions in water. **(A)** Cl- vs. Na+, **(B)** Ca^{2+} vs. SO_4^{2-}, **(C)** Ca^{2+} vs. HCO_3^-, **(D)** (Ca^{2+}+Mg^{2+}) vs. (HCO_3^- + SO_4^{2-}), and **(E)** (Na^++K^+)-Cl^- vs. (Ca^{2+}+Mg^{2+})-(SO_4^{2-} + HCO_3^-).

river water and Cuopu Lake are derived from the dissolution of carbonate minerals.

The origin of Ca^{2+}, Mg^{2+}, HCO_3^-, and SO_4^{2-} in groundwater can be reflected from the molar ratio of (Ca^{2+} + Mg^{2+}) to (HCO_3^- + SO_4^{2-}) in water. Specifically, a molar ratio of 1:1 indicates that these ions are obtained from the dissolution of carbonate rocks and sulfate minerals, a molar ratio of greater than 1:1 indicates that ion exchange process dominates (**Eq. 3**), and a molar ratio of less than 1:1 indicates the presence of reverse ion exchange (**Eq. 4**). As shown in plot of (Ca^{2+} + Mg^{2+}) versus (HCO_3^- + SO_4^{2-}) of the water samples (**Figure 6D**), the samples of river water and Cuopu Lake are distributed along the line with a slope of 1:1, while the water samples of the geothermal water are distributed below the line. Meanwhile, the concentration of Ca^{2+} is far higher than that of Mg^{2+} in the geothermal water. Therefore, it can be inferred that the relatively depleted Ca^{2+} in the geothermal water may be affected by ion exchange (**Eq. 3**), which is caused by silicate weathering.

In the diagram of (Na^+ + K^+)-Cl^- versus (Ca^{2+} + Mg^{2+})-(SO_4^{2-} + HCO_3^- + CO_3^{2-}) (**Figure 6E**), all samples are essentially distributed along a 1:1 line. These results indicate that the hydrochemical processes of the geothermal water and the surface water are mainly controlled by cation exchanges and adsorption in the dissolution of silicate minerals (Li et al., 2020).

TABLE 2 | Rare Earth element composition of geothermal water in the study area (ug/L).

Sample	Location	La	Ce	Pr	Nd	Sm	Eu	Gd	Tb	Dy
BT13	Rekeng	0.05	0.17	0.007	0.021	0.004	0.017	0.005	0.004	0.002
BT14	Rekeng	0.03	0.3	0.004	0.016	0.001	0.008	0.002	0.004	0.004
BT15	Rekeng	0.034	0.13	0.005	0.007	0.002	0.008	0.003	0.004	0.005
BT18	Rekeng	0.021	0.12	0.006	0.008	0.005	0.006	0.002	0.004	0.005
BT20	Rekeng	0.054	0.18	0.007	0.028	0.0035	0.008	0.0035	0.004	0.0025
BT23	Reshuitang	0.036	0.14	0.004	0.011	0.002	0.015	0.002	0.004	0.003
BT24	Reshuitang	0.061	0.18	0.007	0.034	0.009	0.01	0.004	0.004	0.001
BT25	Reshuitang	0.059	0.17	0.009	0.03	0.008	0.014	0.006	0.0005	0.002
BT26	Reshuitang	0.11	0.26	0.017	0.067	0.013	0.008	0.015	0.003	0.009
BT27	Reshuitang	0.032	0.13	0.004	0.009	0.004	0.022	0.006	0.003	0.008
CPH	Cuopu Lake	0.018	0.093	0.001	0.004	—	—	—	—	—
RW	Baqu River	0.078	0.16	0.007	0.028	0.003	0.007	0.005	0.004	0.005
Sample	Ho	Er	Tm	Yb	Lu	∑REE	LREE/HREE	(La/Yb)N	δCe	δEu
BT13	0.003	0.002	0.004	0.003	0.006	0.298	9.28	1.61	1.98	16.69
BT14	0.003	0.003	0.004	0.003	0.006	0.388	12.38	0.97	5.96	24.84
BT15	0.003	0.004	0.004	0.005	0.006	0.22	5.47	0.66	2.17	14.34
BT18	0.003	0.003	0.004	0.005	0.006	0.198	5.19	0.41	2.33	8.33
BT20	0.0025	0.0025	—	0.0045	—	0.3	14.38	1.16	2.02	10.04
BT23	0.003	0.002	0.003	0.003	0.005	0.233	8.32	1.16	2.54	32.93
BT24	0.003	0.002	0.004	0.002	0.005	0.326	12.04	2.95	1.90	7.32
BT25	0.002	0.002	0.004	0.003	0.005	0.3145	12.08	1.91	1.61	8.87
BT26	0.002	0.029	0.003	0.007	0.005	0.548	6.51	1.52	1.31	2.52
BT27	0.001	0.005	0.003	0.004	0.005	0.236	5.74	0.78	2.50	19.72
CPH	—	—	—	—	—	0.116		—	4.77	—
RW	0.002	0.003	0.003	0.002	0.005	0.312	9.76	3.78	1.49	7.94

Cation exchanges and adsorption in the geothermal water result in a decrease in Ca^{2+} and Mg^{2+} concentrations and an increase in Na^{+} concentration (**Figure 3**, Wang et al., 2021). According to the molar ratio diagrams of the major ions in water, the hydrochemical processes in the study area are mainly controlled by the dissolution of silicate minerals.

$$CaSO_4 \cdot 2H_2O \leftrightharpoons Ca^{2+} + SO_4^{2-} + 2H_2O \quad (1)$$

$$CaCO_3 + H_2CO_3 \rightarrow Ca^{2+} + 2HCO^{3-} \quad (2)$$

$$Ion\ exchange:\ 2Na^{+} - Clay + Ca^{2+} \rightarrow 2Na^{+} + Ca^{2+} - Clay_2 \quad (3)$$

$$Reverse\ ion\ exchange:\ 2Na^{+} + Ca^{2+} - Clay_2 2Na^{+} - Clay + Ca^{2+} \rightarrow 2Na^{+} - Clay + Ca^{2+} \quad (4)$$

Characteristics and Controlling Factors of Rare Earth Element Contents in Geothermal Water

The composition of REEs in geothermal water in the study area is shown in **Table 2**. The contents of REEs (except for Yttrium) in the Chaluo hot springs are lower than those of the hot springs around the Kangding area in western Sichuan Province. They are 0.306 ± 0.103 ug/L and 0.669 ± 0.367 ug/L, respectively (Zhang, 2018b). In addition, the water in the Cuopu Lake has low REE contents, while the river water has high REE contents. The difference in the REE contents between the surface water and the geothermal water may be related to the material exchanges between water and rocks (Fan et al., 2021).

Studies have shown that REEs in water bodies are derived from the weathering or dissolution of minerals, the reductive dissolution of Fe and Mn oxides in sediments, the leaching and dissolution of secondary minerals, and human activities (Markert and Zhang, 1991; Dia et al., 2000; Tweed et al., 2006; Kynicky et al., 2012). The dominant factors of these REE sources include pH, oxidation-reduction potential (OPR), and mineral adsorption/dissolution (Leybourne et al., 2000; Noack et al., 2014; Gruau et al., 2004; Koeppenkastrop and De Carlo, 1992; Coppin et al., 2002). pH can control the REE contents by directly influencing the chemical weathering or adsorption/precipitation of REE minerals and by indirectly affecting the complexation (Namely, inorganic ions in the water column such as CO_3^{2-}, PO_4^{3-}, F^{-}, SO_4^{2-}, Cl^{-}, NO_3^{-} as ligands combine with rare Earth elements to form complexes) or adsorption of REEs (Millero, 1992; Noack et al., 2014). Generally, there is a close negative correlation between the pH and the REE contents of water bodies (Noack et al., 2014). **Figure 7A** shows almost no correlation between the pH and ∑REE (R^2 = 0.02) of geothermal water in the study area. However, the ∑REE tends to increase with a decrease in pH when pH < 9, and there is a significant positive correlation between the ∑REE and pH (R^2 = 0.84) when pH > 9. These results are consistent with the study of Noack et al. (2014). It is speculated that the adsorption-absorption regulation of REEs decreases as alkalinity increases in the water bodies. Meanwhile, the increase in the dissolution of CO_2 increases ∑REE through complexation reactions (Zhu, 2006; Liu, 2018). OPR can directly affect redox-sensitive REEs such as Ce and Eu and can indirectly affect REEs by influencing the precipitation or dissolution of Fe and Mn oxides/hydroxides (Guo et al., 2010). Fe and Mn oxides/hydroxides adsorb REEs in an oxidizing environment but

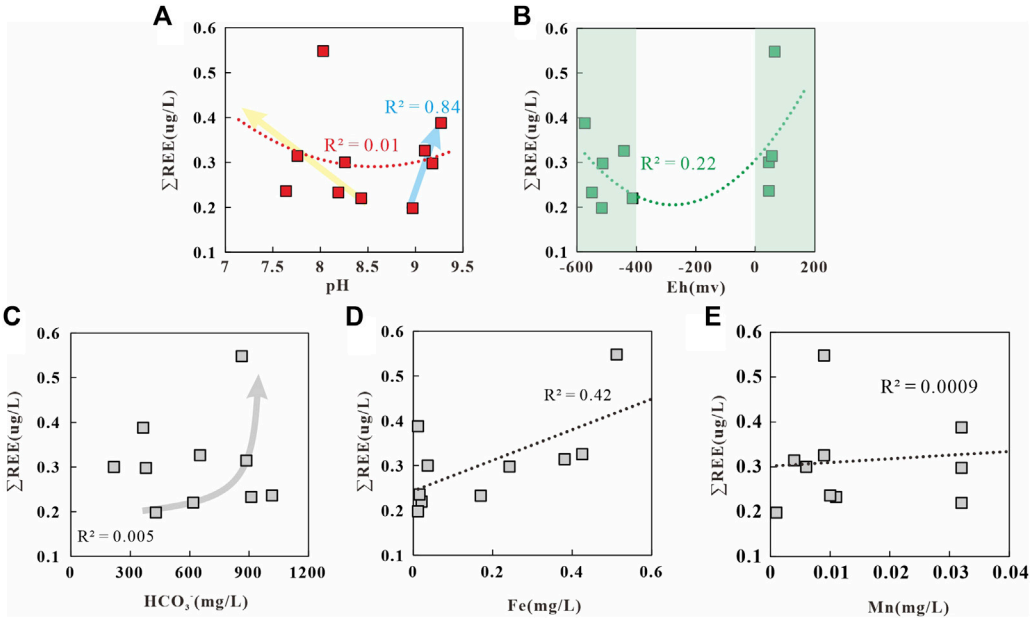

FIGURE 7 | Relationship between ∑REE and pH **(A)**, Eh **(B)**, HCO_3^- **(C)**, Fe **(D)** and Mn **(E)** in the geothermal water of Chaluo.

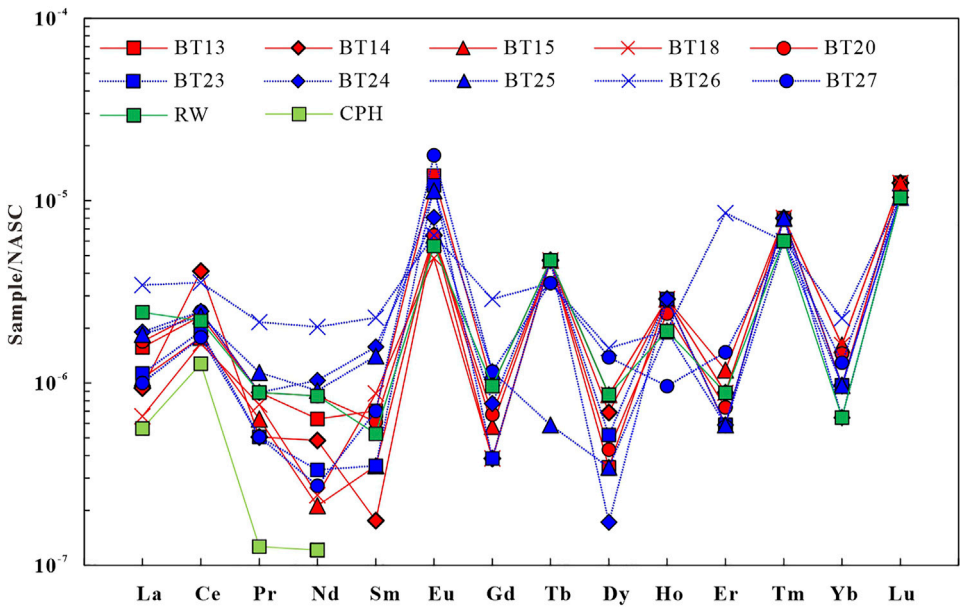

FIGURE 8 | North American shale standardized partitioning pattern of geothermal water and surface water rare Earth elements in the study area.

dissolve and release REEs in a reducing environment. As shown in the diagram of Eh versus ∑REE of the study area (**Figure 7B**), there is essentially no correlation between the Eh and ∑REE, reflecting the fact that REEs are barely influenced by Eh. In alkaline water bodies, HCO_3^- occurs in the form of $LnCO_3^+$ and $Ln(CO_3)_2^-$ after experiencing complexation reactions with REEs (Wood, 1990). **Figure 7C** shows that there is no correlation between HCO_3^- and ∑REE. However, in geothermal water with a high HCO_3^- content, the ∑REE tends to increase with an increase in HCO_3^-. This finding indicates that high HCO_3^- content is favorable for REE enrichment (Xie et al., 2012). In geothermal water with a low HCO_3^- content, however, REEs may be liable to be affected by other factors such as pH. The diagrams of Fe versus ∑REE and Mn versus ∑REE (**Figures 7D,E**) show a certain positive correlation between Fe and ∑REE and no significant correlation between Mn and ∑REE. These results indicate that the reductive dissolution of Fe oxides/

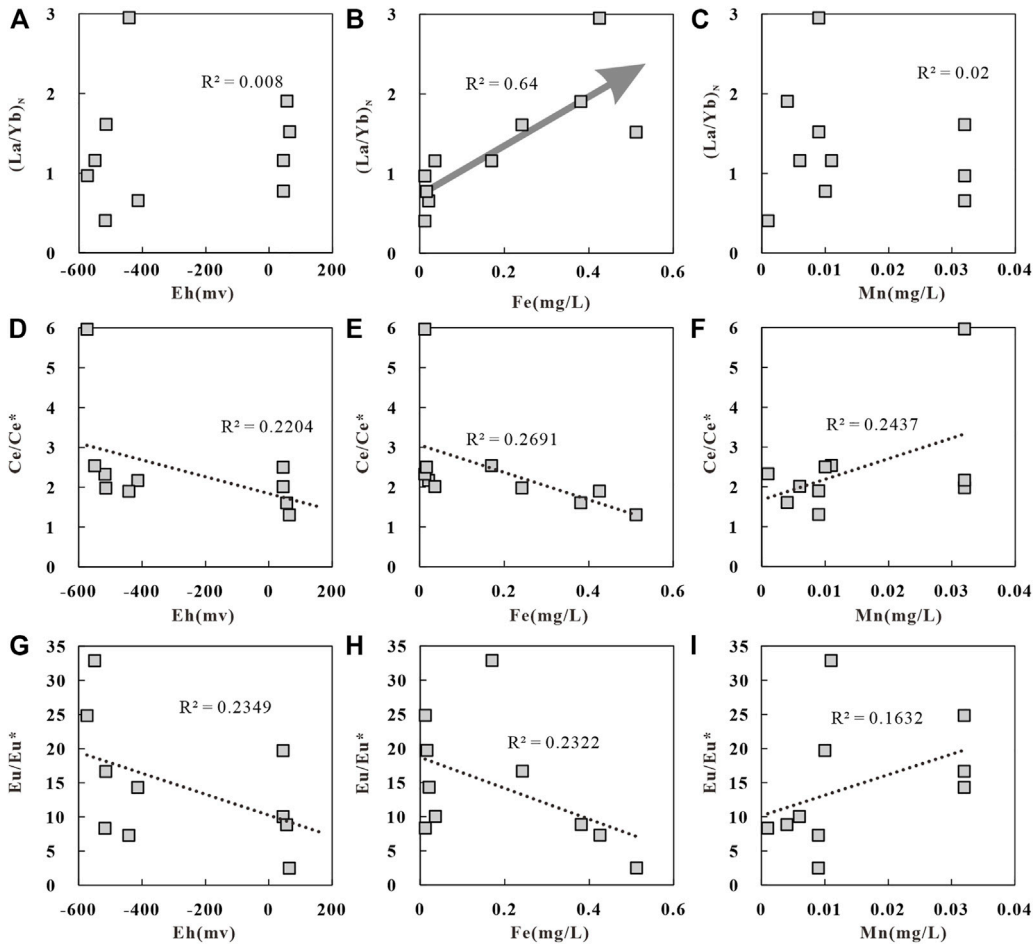

FIGURE 9 | Correlation of geothermal water in the study area, **(A)** $(La/Yb)_N$ versus Eh, **(B)** $(La/Yb)_N$ versus, **(C)** $(La/Yb)_N$ versus Mn, **(D)** Ce/Ce* versus Eh, **(E)** Ce/Ce* versus, **(F)** Ce/Ce* versus Mn, **(G)** Eu/Eu* versus Eh, **(H)** Eu/Eu* versus, **(I)** Eu/Eu* versus Mn.

hydroxides in geothermal water accounts for the increase in the REE content. Overall, the REE contents depend on the reductive dissolution of Fe oxides/hydroxides, followed by pH.

Rare Earth Element Fractionation in Geothermal Water and Controlling Factors

The North American Shale Composite (NASC) (Haskin et al., 1968) normalized REE patterns of the geothermal water in the study area (**Figure 8**) take the shape of gentle sawteeth (Haley et al., 2004). The LREE(La-Eu)/HREE(Gd-Lu) ratio of geothermal water varies from 5.19 to 14.38. The $(La/Yb)_N$ ratio is generally used to replace the LREE(La-Eu)/HREE(Gd-Lu) ratio to characterize the relative enrichment of LREEs in geothermal water (Zhao Y. Y. et al., 2019). The $(La/Yb)_N$ ratio of the geothermal water in the study area is 0.41–2.95, with an average of 1.31, reflecting the enrichment of LREEs. **Figure 9A** shows no significant correlation between Eh and $(La/Yb)_N$, indicating that Eh does not directly affect the REE contents. Studies show that Fe and Mg preferentially adsorb LREEs in the process of oxidation-induced precipitation, leading to the relative enrichment of HREEs. Meanwhile, Fe and Mg oxides will release LREEs after reductive dissolution, leading to a relative enrichment of LREEs in water bodies (Tang and Johanesson, 2010). **Figure 9B** shows a significant positive correlation between Fe and $(La/Yb)_N$. That is, as the Fe content increases, $(La/Yb)_N$ increases significantly and gradually and the REE fractionation enhances. In contrast, **Figure 9C** shows that this is almost no correlation between Mn and $(La/Yb)_N$. These occur possibly for the following reasons. Fe and Mg oxides have different absorption capacities of LREEs and HREEs. The Fe concentration is higher than the Mn concentration in the geothermal water, and Fe oxides release more LREEs after reductive dissolution. As a result, the geothermal water is richer in LREEs than in HREEs.

The redox-sensitive Ce and Eu elements are also commonly used to reflect the fractionation of REEs. Ce exists in both +3 and +4 valence states. In an oxidizing environment, Ce^{3+} in water bodies converts into Ce^{4+} after losing electrons, which will be preferentially adsorbed by Fe and Mn oxides and is then separated from other REEs in the +3 valence state, leading to Ce depletion in water bodies. In a reducing environment, adsorbed Ce^{4+} is reduced to Ce^{3+} and enters water bodies due to the dissolution of Fe and Mn oxides, resulting in Ce enrichment (Byrne and Sholkovitz, 1996).

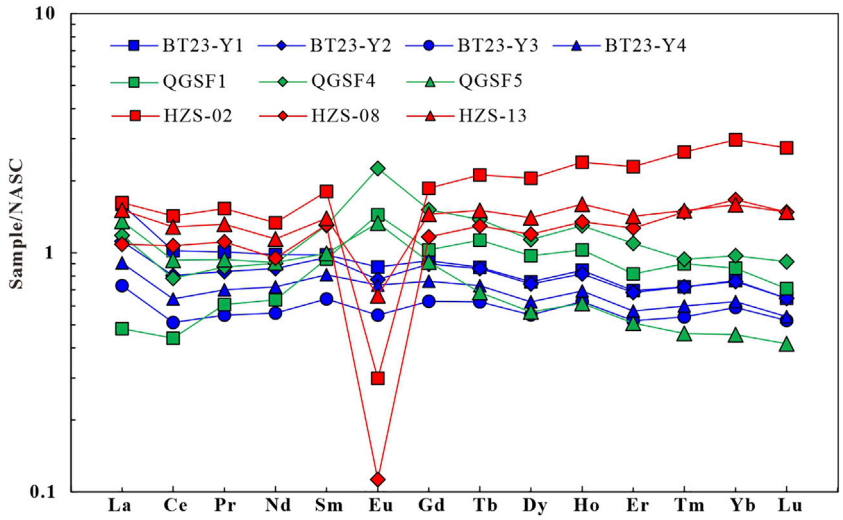

FIGURE 10 | Standardized allotment map of North American shales in the study area rocks (Qugasi Formation data (QGSF1, 4, 5) according to Wang H Y, 2017; HZS data according to Zhang F. Y. et al, 2018).

Eu normally occurs in the Eu^{3+}valence state. In a reducing environment, Eu^{3+} converts into Eu^{2+} after extracting electrons, which will separate from the other REEs in the +3 valence state due to chemical differences, thus resulting in Eu depletion. Among various equations used to calculate Ce/Ce* and Eu/Eu* ratios (Zhao Y. Y. et al., 2019), the following equations (Guo et al., 2010) are used in this study:

$$Ce/_{Ce*} = CeN/_{(LaN*\mathrm{Pr}N)} \cdot 0.5 \quad (5)$$

$$Eu/_{Eu*} = EuN/_{(SmN*GdN)} \cdot 0.5 \quad (6)$$

The Ce/Ce* ratio of the geothermal water in the study area is 1.31–5.96, with an average of 2.43, reflecting positive Ce anomalies. The Eu/Eu* ratio of the geothermal water is 2.52–32.93, with an average of 14.56, indicating positive Eu anomalies. Factors affecting Ce anomalies in water bodies usually include OPR and mineral adsorption/dissolution or the weathering of the surrounding rocks (Elderfield et al., 1990). There is a weak negative correlation between Eh and the Ce/Ce* ratio in the geothermal water in the study area (**Figure 9D**). That is, a lower Eh suggests a higher Ce/Ce* ratio, indicating that the positive Ce anomalies in water bodies are caused by the redox environment. Specifically, Ce^{4+} converts into Ce^{3+} with the dissolution of Fe and Mn oxides, resulting in positive Ce anomalies (Xie et al., 2012). In contrast, **Figure 9E** shows a certain negative correlation between Fe and the Ce/Ce* ratio, and **Figure 9F** shows a certain positive correlation between Mn and the Ce/Ce* ratio. These results indicate that the dissolution of Mn oxides in water bodies leads to positive Ce anomalies.

To further investigate the REE fractionation in water-rock interactions, this study obtained NASC-normalized REEs patterns of the Tumugou and Qugasi formations and Yanshanian granites (**Figure 1C**) in the study area. According to the NASC-normalized REE patterns, the rocks of the Qugasi Formation show positive Eu anomalies (Wang, 2017; **Figure 10**). In contrast, rocks of the Tumugou Formation and especially the Yanshanian granites show negative Eu anomalies (Zhang F. Y. et al., 2018). All types of rocks show slightly negative Ce anomalies, from which it can be inferred that the weathering of surrounding rocks roughly does not cause positive Ce anomalies. The surface water near the geothermal water shows positive Ce anomalies (**Figure 8**), with a Ce/Ce* ratio of 1.49–4.77, with an average of 3.13. This value is slightly higher than the Ce/Ce* ratio of the geothermal water, indicating that the geothermal water may be influenced by the positive Ce anomalies of the surface water (Barrat et al., 2000). Therefore, the positive Ce anomalies in the geothermal water result from both the dissolution of Eh and Mn oxides and surface water. **Table 3**.

TABLE 3 | Rare Earth element composition of geothermal well cores in the study area (ug/g).

Sample	La	Ce	Pr	Nd	Sm	Eu	Gd
BT23-Y1	51	74.5	7.96	32.4	5.58	1.08	4.82
BT23-Y2	35.7	58.6	6.61	28.4	5.44	0.96	4.67
BT23-Y3	23.3	37.3	4.33	18.5	3.66	0.68	3.26
BT23-Y4	29	46.9	5.54	23.8	4.62	0.91	3.96
Sample	Tb	Dy	Ho	Er	Tm	Yb	Lu
BT23-Y1	0.74	4.39	0.88	2.36	0.36	2.37	0.31
BT23-Y2	0.73	4.3	0.85	2.32	0.36	2.35	0.31
BT23-Y3	0.53	3.19	0.65	1.77	0.27	1.83	0.25
BT23-Y4	0.62	3.62	0.72	1.94	0.3	1.94	0.26

The negative correlation between Eh and the Eu/Eu* ratio in the geothermal water (**Figure 9G**) indicates that the positive Eu anomalies in the geothermal water are caused by the reducing environment. Meanwhile, the correlations between Fe and the Eu/Eu* ratio (**Figure 9H**) and between Mn and the Eu/Eu* ratio (**Figure 9I**) indicate that the dissolution of Mn oxides promotes the positive Eu anomalies. As mentioned above, the NASC-normalized

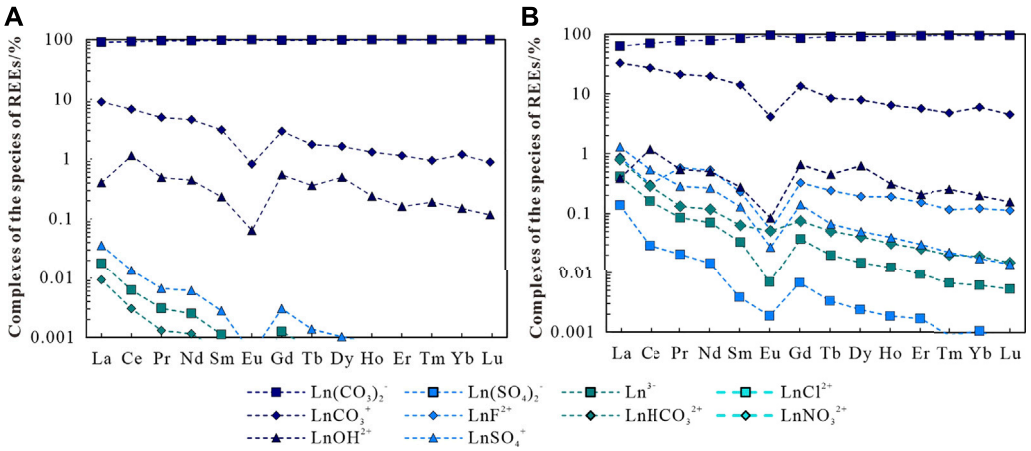

FIGURE 11 | Percentage of each inorganic complexation form of rare Earth elements in geothermal water BT15 **(A)** and BT25 **(B)** in the study area.

REE patterns (**Figure 10**) show that only rocks in the Qugasi Formation show positive Eu anomalies, while the rocks in the Tumugou Formation and Yanshanian granites show negative Eu anomalies. It can be inferred from these results that water-rock interactions between the Qugasi Formation and deep geothermal water also cause positive Eu anomalies. The Eu/Eu^{*} ratio of the surface water is 7.94 and shows significant positive Eu anomalies which indicating positive Eu anomalies in surface water was inherited from the rock of Qugasi Formation (Dong et al., 2017). It is lower than that of the geothermal water, suggesting that the geothermal water is affected by the surface water. In addition, the dissolved feldspar minerals in water bodies also lead to positive Eu anomalies and calcite precipitation (Lee et al., 2003; Liu et al., 2016). The surrounding rocks in the study area are rich in feldspar minerals and the geothermal water in the Batang area is supersaturated with calcite (Zhang, 2020). Therefore, the dissolution of feldspar in the surrounding rocks in the study area promotes the Eu enrichment. Overall, the Eu positive anomalies in the geothermal water result from the combined effects of the reducing environment, surrounding rocks, water bodies, and feldspar dissolution.

Distribution of Rare Earth Element Complexes in Geothermal Water

In this study, the composition and forms of REEs in water sample BT15 from the Rekeng hot springs and the water sample BT25 from the Reshuitang hot springs were determined through

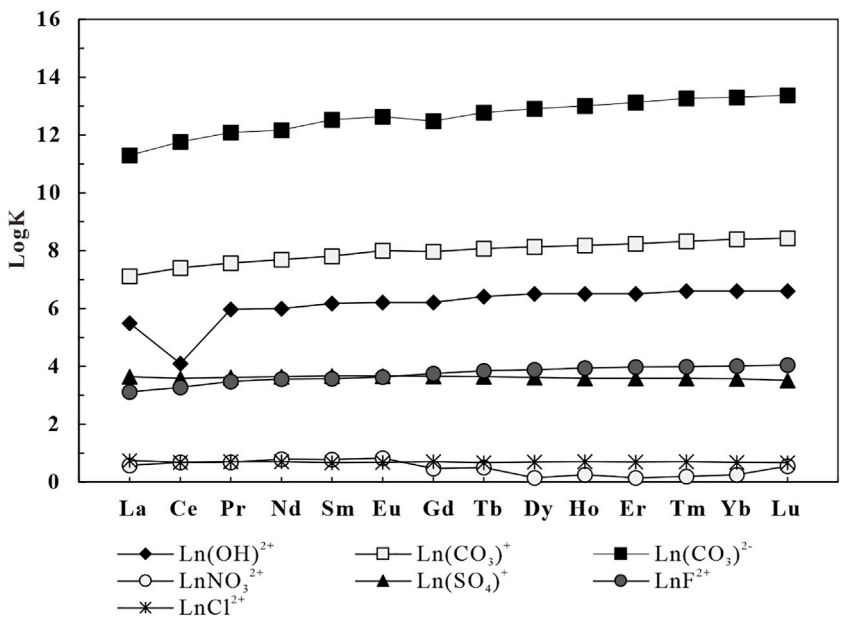

FIGURE 12 | Variation of complexation stability constants of different complexes of rare Earth elements with increasing elemental order (temperature 25°C) (Lee and Byrne, 1992; Millero, 1992; Luo and Byrne, 2001, 2004; Schijf and Byrne, 2004).

calculation and simulation analysis using the Visual MINTEQ 3.0 software. Specifically, measured temperatures, pH, major anions, and REE concentrations were input to MINTEQ to determine the inorganic complex species of REEs in the water samples. The simulation results show that the complex species in the geothermal water mainly include $Ln(CO_3)_2^-$, $LnCO_3^+$, and $LnOH^{2+}$ (Ln signifies the REE). This finding is roughly consistent with the complex species in partially alkaline water bodies (Liu et al., 2021). As shown in **Figure 11**, the inorganic complexes in the Rekeng geothermal water are dominated by $Ln(CO_3)^{2-}$, which accounts for 90.47–99.11% of the total mass concentration of inorganic complexes. They also include $LnCO_3^+$ and $LnOH^{2+}$, which account for 0.82–9.06% and 0.06–1.14%, respectively, and other complexes account for less than 0.01%. The complexes in the Reshuitang geothermal water mainly include $Ln(CO_3)_2^-$ and $LnCO_3^+$, which account for 62.89–95.22% and 4.47–33.18%, respectively. They also include $LnSO_4^+$, which accounts for 0.013–1.31%, and other complexes account for less than 0.1%.

As shown in **Figure 11**, with an increase in the atomic number of the REEs in the geothermal water, the percentage of $Ln(CO_3)_2^-$ gradually increases but the percentages of other complexes such as $LnCO_3^+$ gradually decrease (Liu et al., 2021). This occurs because the stability constants (lgK) of different REE complexes increase as the atomic order of REEs increases. The LgK of $(CO_3)_2^-$is higher than that of other complexes, and therefore the percentage of $Ln(CO_3)_2^-$ increases with an increase in the atomic number of REEs (**Figure 12**).

CONCLUSION

This study determined the hydrochemical characteristics and REE contents of water samples collected from the Chaluo hot springs and rock samples from the surrounding areas through analysis and tests, obtaining the following conclusions:

1) In terms of hydrochemical types of the Chaluo hot springs, the geothermal water is of Na-HCO_3 type, the river water is of mixed Ca-Na-HCO_3 type, and the lake water is of Ca-HCO_3 type. The cations in the geothermal water are mainly controlled by water-rock interactions and evaporation, the anions are primarily determined by water-rock interactions, and the hydrochemical composition of the surface water is controlled by water-rock interactions. Overall, the hydrochemical processes in the water bodies of the study area are mainly controlled by the dissolution of silicate minerals.
2) The total REE content in the geothermal water is 0.306 ± 0.103 ug/L. Studies reveal that the REE contents are primarily affected by the reductive dissolution of Fe oxides/hydroxides, followed by pH.
3) The LREE/HREE and $(La/Yb)_N$ ratios of the geothermal water are 5.19–14.38 and 0.41 to 2.95, respectively, indicating the relative enrichment of LREEs. They are mainly affected by Fe oxides. In addition, the geothermal water shows positive Eu and Ce anomalies, which are caused by both the dissolution of Eh and Mn oxides and surface water. Furthermore, the water-rock interactions between the Qugasi Formation and deep geothermal water also contribute to the positive Eu anomalies.
4) According to the results of the calculation and simulation analysis using the Visual MINTEQ 3.0 software, the complex species of REEs in the geothermal water mainly include $Ln(CO_3)_2^-$, $LnCO_3^+$, and $LnOH^{2+}$. This finding is roughly consistent with the complex species of REEs in alkaline water and is caused by the stability constants of complexation reactions.

DATA AVAILABILITY STATEMENT

The original contributions presented in the study are included in the article/Supplementary Material, further inquiries can be directed to the corresponding author.

AUTHOR CONTRIBUTIONS

SW: Drafting the manuscript, analysis and interpretation of data. FL: Acquisition of data. WZ: Analysis and interpretation of data. HZ: Acquisition of data. RY: Verify data. YL: Participate in mapping. XY: Check the manuscript.

FUNDING

This study was financially supported by the grants from the geothermal survey project of the China Geological Survey (Grant No. DD20190128) and basic Research Operations Project of the Institute of Hydrogeology and Environmental Geology, Chinese Academy of Geological Sciences (SK202212).

REFERENCES

Barrat, J. A., Boulègue, J., Tiercelin, J. J., and Lesourd, M. (2000). Strontium Isotopes and Rare-Earth Element Geochemistry of Hydrothermal Carbonate Deposits from Lake Tanganyika, East Africa. *Geochimica et Cosmochimica Acta* 64 (2), 287–298. doi:10.1016/s0016-7037(99)00294-x

Byrne, R. H., and Sholkovitz, E. R. (1996). "Chapter 158 Marine Chemistry and Geochemistry of the Lanthanides," in *Handbook on the Physics and Chemistry of Rare Earth*. Editors K. A. Gschneidner and L. Eyring (Amsterdam: Elsevier), 497–593. doi:10.1016/s0168-1273(96)23009-0

Cao, R. W., Zhou, X., Chen, B. H., and Li, Z. (2021). Hydrogeochemical Characteristics and Genetic Analysis of the Chaluo hot springs and Geysers in the Batang County of Sichuan Province. *Earth Sci. Front.* 28 (4), 361–372. doi:10.13745/j.esf.sf.2020.6.35

Coppin, F., Berger, G., Bauer, A., Castet, S., and Loubet, M. (2002). Sorption of Lanthanides on Smectite and Kaolinite. *Chem. Geology.* 182 (1), 57–68. doi:10.1016/s0009-2541(01)00283-2

Dewey, B. J. F., Shackleton, R. M., Chang, C. F., and Sun, Y. Y. (1988). The Tectonic Evolution of the Tibetan Plateau. *Phil Trans. R. Soc. Lond.* 327, 379–413.

Dia, A., Gruau, G., Olivié-Lauquet, G., Riou, C., Molénat, J., and Curmi, P. (2000). The Distribution of Rare Earth Elements in Groundwaters: Assessing the Role

of Source-Rock Composition, Redox Changes and Colloidal Particles. *Geochimica et Cosmochimica Acta* 64 (24), 4131–4151. doi:10.1016/s0016-7037(00)00494-4

Dong, L. X., Jiang, Y. B., Zhang, H. Y., Ji, H. B., Wu, Y. K., Wang, P., et al. (2017). Geochemistry of Dissolved Rare Earth Elements in Watershed at Northern Mount Huangshan Landscape. *J. Chin. Soc Rare Earth* 35 (2), 283–293. doi:10.11785/S1000-4343.20170216

Elderfield, H., Upstill-Goddard, R., and Sholkovitz, E. R. (1990). The Rare Earth Elements in Rivers, Estuaries, and Coastal Seas and Their Significance to the Composition of Ocean Waters. *Geochimica et Cosmochimica Acta* 54 (4), 971–991. doi:10.1016/0016-7037(90)90432-k

Fan, L. J., Zou, S. Z., Xie, Q. L., Lu, L., Lin, Y. S., and Pei, J. G. (2021). Rare Earth Element Geochemical Characteristics of Karst Groundwater in Heqing Basin, Yunnan Province. *J. Chin. Soc Rare Earth* 39 (5), 805–815. doi:10.11785/S1000-4343.20210514

Fan, Y., Pang, Z., Liao, D., Tian, J., Hao, Y., Huang, T., et al. (2019). Hydrogeochemical Characteristics and Genesis of Geothermal Water from the Ganzi Geothermal Field, Eastern Tibetan Plateau. *Water* 11 (8), 1631. doi:10.3390/w11081631

Fu, G. H., and Yin, J. C. (2009). A Study on the Distribution and General Mechanism about the Hot spring as Well as Tourism Development in Ganzi of Sichuan Province. *J. Northwest. Univ. (Nat Sci. Ed.* 1, 148–154. doi:10.16152/j.cnki.xdxbzr.2009.01.047

Gibbs, R. J. (1970). Mechanisms Controlling World Water Chemistry. *Science* 170, 1088–1090. doi:10.1126/science.170.3962.1088

Göb, S., Loges, A., Nolde, N., Bau, M., Jacob, D. E., and Markl, G. (2013). Major and Trace Element Compositions (Including REE) of mineral, thermal, Mine and Surface Waters in SW Germany and Implications for Water-Rock Interaction. *Appl. Geochem.* 33, 127–152. doi:10.1016/j.apgeochem.2013.02.006

Goldstein, S. J., and Jacobsen, S. B. (1988). Rare Earth Elements in River Waters. *Earth Planet. Sci. Lett.* 89 (1), 35–47. doi:10.1016/0012-821x(88)90031-3

Gruau, G., Dia, A., Olivié-Lauquet, G., Davranche, M., and Pinay, G. (2004). Controls on the Distribution of Rare Earth Elements in Shallow Groundwaters. *Water Res.* 38 (16), 3576–3586. doi:10.1016/j.watres.2004.04.056

Guo, H., Zhang, B., Wang, G., and Shen, Z. (2010). Geochemical Controls on Arsenic and Rare Earth Elements Approximately along a Groundwater Flow Path in the Shallow Aquifer of the Hetao Basin, Inner Mongolia. *Chem. Geol.* 270 (1-4), 117–125. doi:10.1016/j.chemgeo.2009.11.010

Guo, Y., Wei, J. C., Gui, H., Zhang, Z., and Hu, M. (2020). Evaluation of Changes in Groundwater Quality Caused by a Water Inrush Event in Taoyuan Coal Mine, China. *Environ. Earth Sci.* 79 (24), 1–15. doi:10.1007/s12665-020-09243-5

Haley, B. A., Klinkhammer, G. P., and McManus, J. (2004). Rare Earth Elements in Pore Waters of marine Sediments. *Geochimica et Cosmochimica Acta* 68 (6), 1265–1279. doi:10.1016/j.gca.2003.09.012

Haskin, L. A., Haskin, M. A., Frey, F. A., and Wildeman, T. R. (1968). Relative and Absolute Terrestrial Abundances of the Rare Earths. *Origin and Distribution of the Elements*, 889–912. doi:10.1016/b978-0-08-012835-1.50074-x

Hederson, P. (1984). "General Geochemical Properities and Abundances of Rare Earth Elements," in *Rare Earth Element Geochemistry*. Editor P. Henderson (Amsterdam: Elsevier), 1–32.

Johannesson, K. H., Stetzenbach, K. J., and Hodge, V. F. (1997). Rare Earth Elements as Geochemical Tracers of Regional Groundwater Mixing. *Geochimica et Cosmochimica Acta* 61 (17), 3605–3618. doi:10.1016/s0016-7037(97)00177-4

Koeppenkastrop, D., and De Carlo, E. H. (1992). Sorption of Rare-Earth Elements from Seawater onto Synthetic mineral Particles: An Experimental Approach. *Chem. Geol.* 95 (3-4), 251–263. doi:10.1016/0009-2541(92)90015-w

Kynicky, J., Smith, M. P., and Xu, C. (2012). Diversity of Rare Earth Deposits: the Key Example of China. *Elements* 8 (5), 361–367. doi:10.2113/gselements.8.5.361

Lee, J. H., and Byrne, R. H. (1992). Examination of Comparative Rare Earth Element Complexation Behavior Using Linear Free-Energy Relationships. *Geochimica et Cosmochimica Acta* 56, 1127–1137. doi:10.1016/0016-7037(92)90050-s

Lee, S.-G., Lee, D.-H., Kim, Y., Chae, B.-G., Kim, W.-Y., and Woo, N.-C. (2003). Rare Earth Elements as Indicators of Groundwater Environment Changes in a Fractured Rock System: Evidence from Fracture-Filling Calcite. *Appl. Geochem.* 18 (1), 135–143. doi:10.1016/s0883-2927(02)00071-9

Leybourne, M. I., Goodfellow, W. D., Boyle, D. R., and Hall, G. M. (2000). Rapid Development of Negative Ce Anomalies in Surface Waters and Contrasting REE Patterns in Groundwaters Associated with Zn-Pb Massive Sulphide Deposits. *Appl. Geochem.* 15 (6), 695–723. doi:10.1016/s0883-2927(99)00096-7

Li, J., Yang, G., Sagoe, G., and Li, Y. (2018). Major Hydrogeochemical Processes Controlling the Composition of Geothermal Waters in the Kangding Geothermal Field, Western Sichuan Province. *Geothermics* 75, 154–163. doi:10.1016/j.geothermics.2018.04.008

Li, X., Huang, X., Liao, X., and Zhang, Y. (2020). Hydrogeochemical Characteristics and Conceptual Model of the Geothermal Waters in the Xianshuihe Fault Zone, Southwestern China. *Ijerph* 17 (2), 500. doi:10.3390/ijerph17020500

Liu, H., Guo, H., Xing, L., Zhan, Y., Li, F., Shao, J., et al. (2016). Geochemical Behaviors of Rare Earth Elements in Groundwater along a Flow Path in the North China Plain. *J. Asian Earth Sci.* 117, 33–51. doi:10.1016/j.jseaes.2015.11.021

Liu, H. Y. (2018). *Distribution of Groundwater Rare Earth Elements in the Typical Region of the North China Plain and Modeling Study on Their Complexation with Iron and Manganese*. Beijing: China University of Geosciences.

Liu, H. Y., Liu, M. H., Zhang, W. M., Sun, Z. X., Wang, Z., Wu, T. H., et al. (2021). Distribution and Fractionation of Rare Earth Elements in High-Fluoride Groundwater from the North China Plain. *Earth Sci. Front* 117, 1–16. doi:10.13745/j.esf.sf.2021.7.24

Luo, L., L. (1994). Inquisition of the Distribution and Cause of the Hot Springs in Western Sichuan. *J. Chongqing Teach. Coll. (Nat Sci. Ed.* 11 (2), 39–47.

Luo, Y.-R., and Byrne, R. H. (2004). Carbonate Complexation of Yttrium and the Rare Earth Elements in Natural Waters. *Geochimica et Cosmochimica Acta* 68, 691–699. doi:10.1016/s0016-7037(03)00495-2

Luo, Y.-R., and Byrne, R. H. (2001). Yttrium and Rare Earth Element Complexation by Chloride Ions at 25°C. *J. Solution Chem.* 30 (9), 837–845. doi:10.1023/a:1012292417793

Markert, B., and Deli, Z. (1991). Natural Background Concentrations of Rare-Earth Elements in a forest Ecosystem. *Sci. Total Environ.* 103 (1), 27–35. doi:10.1016/0048-9697(91)90350-n

Ménager, M., Menet, C., Petit, J., Cathelineau, M., and Côme, B. (1992). Dispersion of U, Th, and REE by Water-Rock Interaction Around an Intragranitic U-Vein, Jalerys Mine, Morvan, France. *Appl. Geochem.* 7, 239–252.

Millero, F. J. (1992). Stability Constants for the Formation of Rare Earth-Inorganic Complexes as a Function of Ionic Strength. *Geochimica et Cosmochimica Acta* 56, 3123–3132. doi:10.1016/0016-7037(92)90293-r

Möller, P. (2000). "Rare Earth Elements and Yttrium as Geochemical Indicators of the Source of mineral and thermal Waters," in *Hydrogeology of Crystalline Rocks*. Editors I. Stober and K. Bucher (Dordrecht, Netherlands: Kluwer Academic Publishers), 227–246.

Moon, S., Huh, Y., Qin, J., and van Pho, N. (2007). Chemical Weathering in the Hong (Red) River basin: Rates of Silicate Weathering and Their Controlling Factors. *Geochimica et Cosmochimica Acta* 71 (6), 1411–1430. doi:10.1016/j.gca.2006.12.004

Noack, C. W., Dzombak, D. A., and Karamalidis, A. K. (2014). Rare Earth Element Distributions and Trends in Natural Waters with a Focus on Groundwater. *Environ. Sci. Technol.* 48, 4317–4326. doi:10.1021/es4053895

Piper, A. M. (1994). A Graphic Procedure in the Geochemical Interpretation of Water-Analyses. *T-am Geophys. Union* 25, 914–928.

Royden, L. H., Burchfiel, B. C., and van der Hilst, R. D. (2008). The Geological Evolution of the Tibetan Plateau. *Science* 321, 1054–1058. doi:10.1126/science.1155371

Sanada, T., Takamatsu, N., and Yoshiike, Y. (2006). Geochemical Interpretation of Long-Term Variations in Rare Earth Element Concentrations in Acidic Hot spring Waters from the Tamagawa Geothermal Area, Japan. *Geothermics* 35 (2), 141–155. doi:10.1016/j.geothermics.2006.02.004

SBGMR (Bureau of Geology and Mineral Resource of Sichuan Province) (1991). *Regional Geology of Sichuan Province*. Beijing: Geological Publishing House.

Schijf, J., and Byrne, R. H. (2004). Determination of SO4β1 for Yttrium and the Rare Earth Elements at I = 0.66 M and T = 25°C-Implications for YREE Solution Speciation in Sulfate-Rich Waters. *Geochimica et Cosmochimica Acta* 68 (13), 2825–2837. doi:10.1016/j.gca.2003.12.003

Tang, J., and Johannesson, K. H. (2010). Rare Earth Elements Adsorption onto Carrizo Sand: Influence of strong Solution Complexation. *Chem. Geology.* 279, 120–133. doi:10.1016/j.chemgeo.2010.10.011

Tang, X., Zhang, J., Pang, Z., Hu, S., Tian, J., and Bao, S. (2017). The Eastern Tibetan Plateau Geothermal belt, Western China: Geology, Geophysics, Genesis, and Hydrothermal System. *Tectonophysics* 717, 433–448. doi:10.1016/j.tecto.2017.08.035

Tong, W., and Zhang, M. T. (1989). *Geothermal Resources in Tengchong*. Beijing: Science Press.

Tong, W., Zhang, M. T., Zhang, Z. F., Liao, Z. J., You, M. Z., Zhu, M. X., et al. (1981). *Geothermal Resources in Tibet*. Beijing: Science Press.

Tweed, S. O., Weaver, T. R., Cartwright, I., and Schaefer, B. (2006). Behavior of Rare Earth Elements in Groundwater during Flow and Mixing in Fractured Rock Aquifers: an Example from the Dandenong Ranges, Southeast Australia. *Chem. Geol.* 234 (3), 291–307. doi:10.1016/j.chemgeo.2006.05.006

Wang, H. Y. (2017). *Geological Characteristics Study of the Qugasi Formation in Baisong-Bendu Area, Sichuan Province*. Chengdu: Chengdu University of Technology.

Wang, Z., Guo, H. M., Xing, S. P., and Liu, H. Y. (2021). Hydrogeochemical and Geothermal Controls on the Formation of High Fluoride Groundwater. *J. Hydrol.* 598. doi:10.1016/j.jhydrol.2021.126372

Wood, S. A., and Shannon, W. M. (2003). Rare-earth Elements in Geothermal Waters from Oregon, Nevada, and California. *J. Solid State. Chem.* 171 (1), 246–253. doi:10.1016/s0022-4596(02)00160-3

Wood, S. A. (1990). The Aqueous Geochemistry of the Rare-Earth Elements and Yttrium. *Chem. Geology.* 82, 159–186. doi:10.1016/0009-2541(90)90080-q

Xie, X. J., Wang, Y. X., Li, J. X., Su, C. L., Wu, Y., Yu, Q., et al. (2012). Characteristics and Implications of Rare Earth Elements in High Arsenic Groundwater from the Datong Basin. *Earth Sci-j China Univ. Geosci.* 37 (2), 381–390.

Xu, X. W., Zhang, P. Z., Wen, X. Z., Qin, Z. L., Chen, G. H., and Zhu, A. L. (2005). Characteristics of Active Tectonics and Models of Earthquake Recurrence in Western Sichuan. *Seismol Geol.* 27 (3), 446–461.

Xu, Z. Q., Hou, L. W., Wang, Z. X., Fu, X. F., and Huang, M. H. (1992). *Orogeic Processes of the Songpan-Ganze Orogenic belt of China*. Beijing: Geological Publishing House.

Xu, Z. Q., Yang, J. S., Li, H. B., Ji, S. C., Zhang, Z. M., and Liu, Y. (2011). On the Tectonics of the India-Asia Collision. *Acta Geol. Sin* 85 (1), 1–33.

Yan, B., and Lin, A. (2015). Systematic Deflection and Offset of the Yangtze River Drainage System along the Strike-Slip Ganzi-Yushu-Xianshuihe Fault Zone, Tibetan Plateau. *J. Geodynamics* 87, 13–25. doi:10.1016/j.jog.2015.03.002

Yuan, J. F., Deng, G. S., Xu, F., Tang, Y. Q., and Li, P. Y. (2017). Hydrogeochemical Characteristics of Groundwater in the Xide Geothermal Field, Southwest Sichuan, China. *Geoscience* 31 (1), 200–208.

Zhang, F. Y., Lai, S. C., and Qin, J. F. (2018c). Petrogenesis and Geological Significance of the Late Cretaceous Haizishan Monzogranite from the Yidun Island Arc. *Geol. J. China Univ.* 24 (3), 340–352. doi:10.16108/j.issn1006-7493.2017129

Zhang, Jian., Li, W. Y., Tang, X. C., Tian, J., Wang, Y. C., Guo, Q., et al. (2017a). Geothermal Data Analysis at the High-Temperature Hydrothermal Area in Western Sichuan. *Sci. China Earth Sci.* 47 (8), 899–915. doi:10.1007/s11430-016-9053-2

Zhang, K., Zhang, Y., Tang, X., and Xia, B. (2013). Late Mesozoic Tectonic Evolution and Growth of the Tibetan Plateau Prior to the Indo-Asian Collision. *Earth-sci Rev.* 114 (3-4), 236–249.

Zhang, W. (2020). *The Formation and Geochemical Response Mechanism of Medium-High Temperature Geothermal System in Western Sichuan*. Beijing: Chinese Academy of Geological Sciences.

Zhang, W., Wang, G., Xing, L., Li, T., and Zhao, J. (2019). Geochemical Response of Deep Geothermal Processes in the Litang Region, Western Sichuan. *Energy Exploration & Exploitation* 37 (2), 626–645. doi:10.1177/0144598718812550

Zhang, Y.-Z., Replumaz, A., Leloup, P. H., Wang, G.-C., Bernet, M., van der Beek, P., et al. (2017b). Cooling History of the Gongga Batholith: Implications for the Xianshuihe Fault and Miocene Kinematics of SE Tibet. *Earth Planet. Sci. Lett.* 465, 1–15. doi:10.1016/j.epsl.2017.02.025

Zhang, Y. H. (2018b). *Research on Genesis and Development of the Geothermal System in the Kangding-Moxi Segment of the Xianshuihe Fault*. Chengdu: Chengdu University of Technology.

Zhang, Y., Xu, M., Li, X., Qi, J., Zhang, Q., Guo, J., et al. (2018a). Hydrochemical Characteristics and Multivariate Statistical Analysis of Natural Water System: A Case Study in Kangding County, Southwestern China. *Water* 10 (1), 80. doi:10.3390/w10010080

Zhao, J. Y., Zhao, W., Zhang, H. X., Qu, Z. W., Li, M., and Yue, G. F. (2019a). Hydrogeochemical Characteristics and Genesis of the Geothermal fields in Batang of Sichuan. *Hydrogeol Eng. Geol.* 46 (4), 81–89. doi:10.16030/j.cnki.issn.1000-3665.2019.04.11

Zhao, Y. Y., Li, S. Z., Li, D., Guo, L. L., Dai, L. M., and Tao, J. L. (2019b). Rare Earth Element Geochemistry of Carbonate and its Paleoenvironmental Implications. *Geotectonica et Metallogenia* 43 (1), 141–167. doi:10.16539/j.ddgzyckx.2019.01.011

Zhu, Z. Z. (2006). *The Geochimal Character and Environmental Effect of Rare Earth Elements in Lakes, Upper and Lower Reaches of Yangtze River, China*. Guiyang: Institute of Geochemistry Chinese Academy of Sciences.

Conflict of Interest: The authors declare that the research was conducted in the absence of any commercial or financial relationships that could be construed as a potential conflict of interest.

Publisher's Note: All claims expressed in this article are solely those of the authors and do not necessarily represent those of their affiliated organizations, or those of the publisher, the editors and the reviewers. Any product that may be evaluated in this article, or claim that may be made by its manufacturer, is not guaranteed or endorsed by the publisher.